Crystal structure of SULT2A3, human hydroxysteroid sulfotransferase

Lars C. Pedersen[1], Evgeniy V. Petrotchenko[1], Masahiko Negishi*

Pharmacogenetics Section, Laboratory of Reproductive and Developmental Toxicology, National Institute of Environmental Health Sciences, National Institutes of Health, Research Triangle Park, NC 27709, USA

Received 21 February 2000; received in revised form 3 April 2000

Edited by Hans Eklund

Abstract The crystal structure of SULT2A3 human hydroxysteroid sulfotransferase has been solved at 2.4 Å resolution in the presence of 3′-phosphoadenosine 5′-phosphate (PAP). The overall structure is similar to those of SULT1 enzymes such as estrogen sulfotransferase and the PAP binding site is conserved, however, significant differences exist in the positions of loops Pro14–Ser20, Glu79–Ile82 and Tyr234–Gln244 in the substrate binding pocket. Moreover, protein interaction in the crystal structure has revealed a possible dimer-directed conformational alteration that may regulate the SULT activity.

Key words: Hydroxysteroid sulfotransferase; Dehydroepiandrosterone; Crystal structure; Sulfation

1. Introduction

Sulfation plays a role in the metabolism, transport and synthesis of steroids. Dehydroepiandrosterone (DHEA) is produced in the adrenals and secreted as a DHEA sulfate (DHEA-S). DHEA-S provides the major source of estrogens that is aromatized in human placenta during pregnancy [1]. The 100-fold higher plasma concentration of DHEA-S over DHEA suggests that DHEA-S is also the main source that may be converted into other steroid hormones in adult peripheral tissues [2,3]. DHEA-S has been reported to have anti-obesity, -aging and -carcinogenic effects [2,3]. A protective effect of DHEA-S against cardiovascular disease is also suggested [2,3]. DHEA sulfation is catalyzed by hydroxysteroid sulfotransferase, an enzyme that transfers the sulfuryl group of the co-factor 3′-phosphate 5′-phosphoadenosine sulfate (PAPS) to the 3-hydroxyl of DHEA [2]. Solving the structure is essential for the development of clinical reagents to target this enzyme.

Cytosolic sulfotransferases or SULTs are divided into two subfamilies. The subfamily 1 (SULT1) includes specific enzymes that sulfate phenolic steroids, whereas subfamily 2 (SULT2) enzymes are characterized by sulfating hydroxysteroids such as DHEA. The structures of mouse estrogen and human catecholamine/dopamine sulfotransferases (SULT1E1 and SULT1A3, respectively) from the SULT1 have been solved [4–6]. In addition, the Golgi-membrane heparan sulfate *N*-sulfotransferase structure has been determined [7,8]. Here we report the first crystal structure of a SULT2 enzyme, human hydroxysteroid sulfotransferase or SULT2A3. The overall structure of SULT2A3 shows striking similarities with the SULT1 enzymes. Significant differences do exist in the substrate binding pocket that may be responsible for high substrate specificity toward hydroxysteroids. The SULT2A3 structure also displays significant contacts between two molecules in the asymmetric unit, which provides motivation for future research on the enzyme dimerization and activity.

2. Materials and methods

2.1. cDNA cloning, expression, purification and crystallization

A SULT2A3 DNA was amplified from a human liver cDNA library using a set of proper primers generated from a published sequence [9] and cloned into pET21a vector (Novagen) using *Nde*I and *Hin*dIII sites. The carboxy-terminal sequence was substituted with Leu_{277}ProArgLysLeuAlaAlaAlaLeuGlu$(His)_6$. The carboxy-terminal His-tagged protein was expressed in *Escherichia coli* BL21DE3 (4 days at 25°C, in 2×YT medium supplemented with 0.25% glucose) and purified using Ni-NTA Agarose (QIAgen). Crystals were grown by mixing equal volumes of SULT2A3 protein at 25 mg/ml in 25 mM HEPES pH 7.5 and 4 mM PAP with 0.8 M citrate and 80 mM cacodylate, titrated to a pH of 5.75. These crystals (0.4×0.4×0.6 mm in size) belong to space group $P2_12_12_1$ with unit cell dimensions of 73.19×96.82×127.38 Å and diffracted to 2.4 Å.

2.2. Crystallographic data collection and structure determination

Data were collected at BNL on beam line x9B on crystals which had been transferred to 0.9 M citrate, 90 mM cacodylate, 4 mM PAP, saturated DHEA and 10% ethylene glycol. Phases for the structure factors were calculated using molecular replacement with the model built from the SULT1E1 (previously known as mEST) coordinates [4]. The SULT2A3 search model contained all backbone atoms of monomer A from the 1AQU coordinates minus residues 84 to 92. Sidechains that are identical between the two structures were included while non-identical sidechains were substituted with serine or alanine residues. Initial attempts to solve the molecular replacement with the synchrotron data set failed. Therefore multiple isomorphous replacement methods were employed. A data set of a crystal soaked in 10 mM trimethyl-lead-acetate was collected on an in house Raxis IV detector. Although these crystals did not appear to be isomorphous to the native data, soaking of the crystals in trimethyl-lead-acetate reduced the mosaicity of the crystal from 1.0 to 0.4. Due to apparently improved crystal packing upon soaking with trimethyl-lead-acetate, molecular replacement using the previous model was attempted on this data set using AMoRe [10]. Peaks 17 and 28 of the rotation function, with correlation coefficients of 7.2 and 6.8, respectively, gave independent correlation coefficients of 19.9 and 20.0 in the translation function. After fitting, these values improved to 28.8 and 28.2 both with independent *R*-factors of 53.4%. When the two solutions were placed at the same origin and refined, the solution gave a combined correlation coefficient of 40.1 with an *R*-factor of 49.7%. After multiple steps of model building and refinement using CNS [11] a final *R*-factor of 21.9% and R_{free} of 25.75% were obtained. This model contained residues A5–A226, A242–A286, B5–B234, B242–B286, PAP for both monomers, 156 waters and six Pb sites. At this point the model (minus waters and Pb atoms) was refined against the native data to 2.4 Å. After multiple stages of manual rebuilding and refinement an *R*-factor of 20.2% and an R_{free} of 23.9% were obtained. This

*Corresponding author. Fax: (1)-919-541 0696.
E-mail: negishi@niehs.nih.gov

[1] Equally contributed.

PII: S0014-5793(00)01479-4

model includes residues A4–A241, A244–A287, B4–B239, B241–B286, both PAP molecules and 185 waters. However, there is no density present for the DHEA package [12]. All data were processed using the Denzo and Scalepack method [13] and all model buildings were carried out by the program 'O' [13] (see Table 1).

3. Results and discussion

3.1. Overall structure and reaction mechanism

The overall structure of SULT2A3 is comprised of a single α/β domain with a five-stranded parallel β sheet that constitutes the PAPS binding site and catalytic center (Fig. 1). A strand–loop–helix motif that contains the PSB-loop (41-TYPKSGT-47) forms specific hydrogen bond interactions with the 5′-phosphate of the PAP molecule. The 3′-phosphate binding site is comprised of interactions from residues along β-strand 8 and α6 helix (Arg121 and Ser129, respectively) as well as backbone interactions with the residues Lys248 and Gly249 near the carboxy-terminal. SULT2A3 appears to catalyze an in-line sulfuryl transfer reaction that has been suggested for other SULT enzymes [14]. His99 and Lys44 of SULT2A3 are in positions to assist in the deprotonation of the acceptor group and the dissociation of the sulfuryl group from PAPS (Fig. 2), as has been proposed for other SULT enzymes [2,3,7,14,15]. Thus, these structural features and reaction mechanisms appear to be well conserved in all SULTs.

3.2. Putative substrate binding site

Residues from α4, α6, α12, β4 and three loops (Pro14–Ser20, Glu79–Ile82 and Asn136–Lys144) constitute the majority of the hydrophobic substrate binding pocket (Fig. 2). In addition, residues from loop Tyr231–Gln244 cover the face of the binding pocket in the SULT2A3 structure. These same secondary structural elements are utilized to form the substrate binding pockets of SULT1E1 and SULT1A3 [4–6], although residues 216–240 are disordered in the latter.

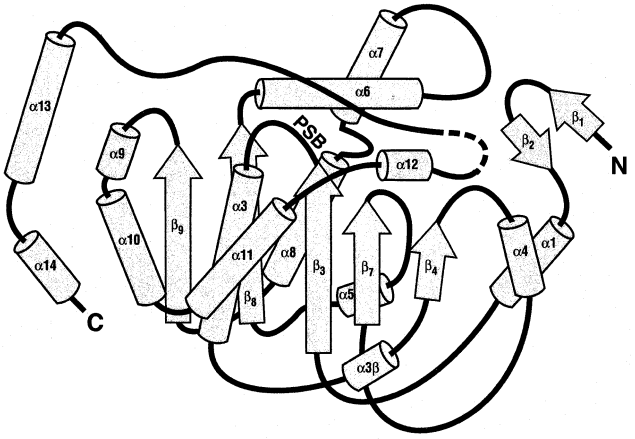

Fig. 1. Topological presentation of the SULT2A3 structure.

The differences between the SULT2A3 and SULT1E1 pockets increase gradually from the catalytic site to the outside of the molecule. There are large differences at the opening of the two pockets (Fig. 3): whereas only four residues (Glu79 to Ile82) constitute a loop forming the opening of SULT2A3, the same loop of SULT1E1 contains nine residues from Glu83 to Asn91 (Fig. 4). In addition, the loops Pro14–Ser20 and Tyr231–Gln244 have collapsed on the opening in the structure

Table 1
Crystallographic data statistics

Data set	Trimethyl-lead-acetate	Native
Unit cell dimensions	$a=72.91$, $b=97.20$, $c=128.44$, $\alpha=90°$, $\beta=90°$, $\delta=90°$	$a=73.19$, $b=96.82$, $c=127.375$, $\alpha=90°$, $\beta=90°$, $\delta=90°$
Space group	$P2_12_12_1$	$P2_12_12_1$
No. of observations	110 204	113 997
Unique reflections	33 275	34 110
R_{sym} (%) (last shell)[a]	5.5% (16.4%)	5.0% (14.3%)
$I/\sigma I$ (last shell)	24.2 (6.0)	15.3 (6.7)
Mosaicity	0.49	1.0
Completeness (%) (last shell)	91.3 (66.4)	94.4 (86.9)
(A) Refinement statistics		
Resolution (Å)	50–2.4	50–2.4
R_{cryst} (%)[b]	21.93	20.2
R_{free}	25.75	23.9
No. of waters	126	185
No. of Pb	6	–
(1) Rms deviation from ideal values		
Bond length (Å)	0.007	0.007
Bond angle (°)	1.2	1.2
Dihedral angle (°)	21.8	21.6
Improper angle (°)	0.81	0.77
Mean B value (Å^b)	45.0	36.9
(2) Ramachandran statistics		
Residues in:		
Most favored regions (%)	91.5	91.1
Additionally allowed regions	7.9	8.9
Generously allowed regions	0.6	0.0
Disallowed regions	0.0	0.0

The coordinates for the final refinement of the SULT2A3 native data set have been submitted to the Protein Data Bank and have the PDB ID code 1EFH.

[a] $R_{sym}=\Sigma(|I-\langle I\rangle|)\Sigma(I)$.

[b] $R_{cryst}=\Sigma||F_o|-|F_c||/\Sigma|F_o|$ calculated from working data set. R_{free} is calculated from 5% of data randomly chosen not to be included in refinement.

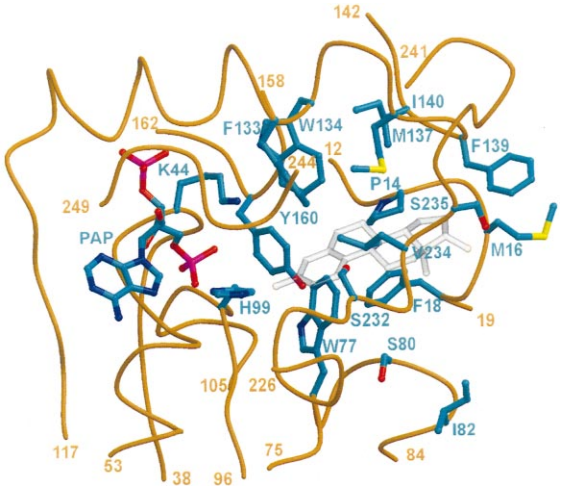

Fig. 2. Active site region of SULT2A3. Residues involved in the catalytic mechanism and residues that line the substrate binding pocket are displayed in dark cyan as is PAP. A semi-transparent model of E2 has been placed in the active site based on the superposition of SULT1E1 to SULT2A3. This figure was created with MOLSCRIPT [18] and Raster3D [19].

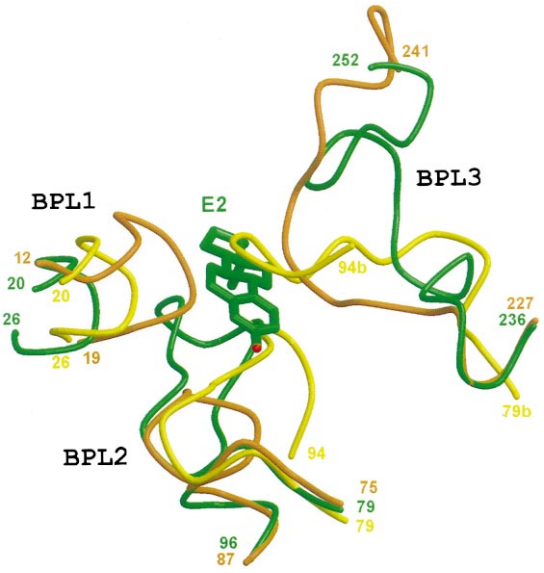

Fig. 3. Superposition of the substrate binding pockets of SULT1E1 (green), SULT1A3 (yellow) and SULT2A3 (brown). The rms for 254 of the most similar Cα's is 1.46 Å^2 for SULT1E1 and 1.36 Å^2 for 205 Cα's for SULT1A3. Residues 79b–94b of SULT1A3 are from the second monomer in the crystallographic dimer. BPL1, BPL2 and BPL3 are the loops that constitute the surface of the substrate binding pocket. This figure was created with MOLSCRIPT [18] and Raster3D [19].

of SULT2A3. As a result, Leu234 of SULT2A3 places its sidechain in direct contact with the E2 molecule in the superposition with the SULT1E1 structure.

Positions of Tyr160, Phe133 and Phe18 in the substrate binding pocket of SULT2A3 superimpose with those of Tyr169, Phe142 and Phe24, respectively, in the SULT1E1 structure. Phe142 and Tyr81 form a substrate-access gate that confers high estrogen specificity to this enzyme and mutations of Tyr81 to a smaller hydrophobic amino acid decreased estrogen and increased activity toward DHEA sulfation [16]. Trp77 of SULT2A3 superimposes with Tyr81 and is in position to form a gate-like structure with Phe133. If, in fact, DHEA binds in the same orientation as E2 in the SULT1E1 structure, conformational alterations of Trp77

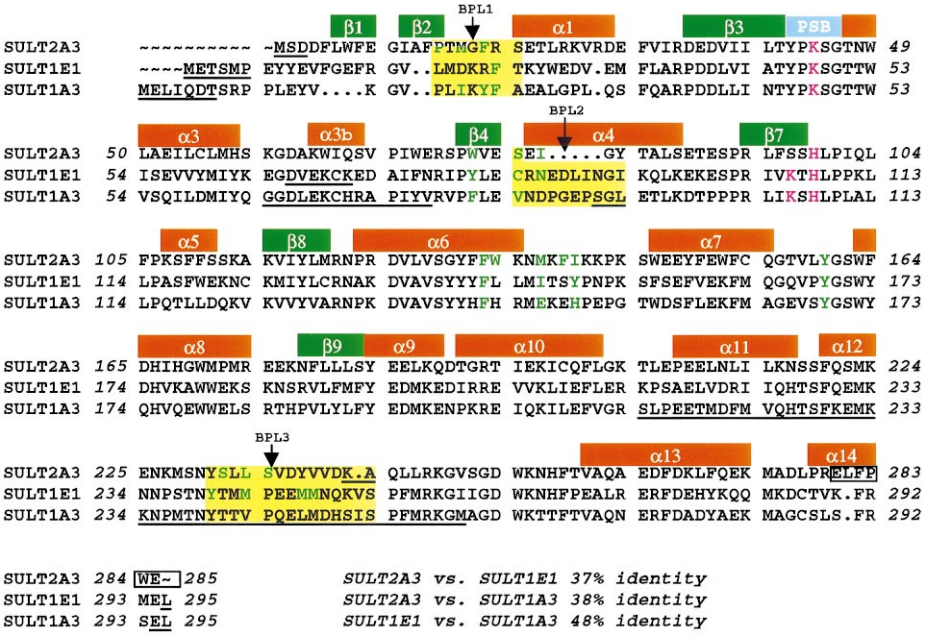

Fig. 4. Sequence alignments of SUTL2A3, SULT1E1 and SULT1A3. Secondary structure elements of SULT2A3 are numbered based upon that previously described for SULT1E1 [4]. In addition, the PSB loop is displayed with a blue box. Residues implicated in the catalytic mechanism are shown in magenta, while those that line the substrate binding pockets are shown in green. The loops that have significant conformational changes between the substrate binding pockets are highlighted in yellow. Underlined residues are not seen in the crystal structures. The carboxy-terminal residues substituted in the crystal structure of SULT2A3 are boxed. BPL1, BPL2 and PBL3 are the loops that constitute the surface of the substrate binding pocket.

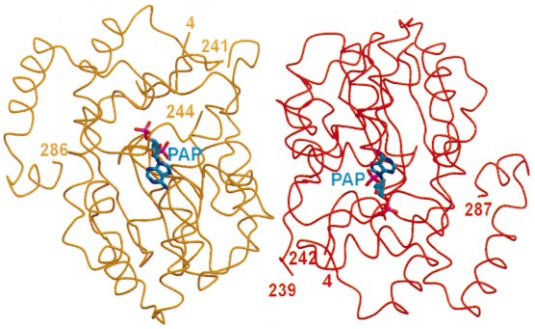

Fig. 5. Crystallographic dimer of SULT2A3. Monomer A is shown in brown and monomer B in red. The PAP molecules are shown in dark cyan. This view demonstrates the near two-fold axis between the two monomers. This figure was created with MOLSCRIPT [18] and Raster3D [19].

and Phe133 as well as of loop Tyr231–Glu244 would be required to accommodate DHEA in the active site. Alternatively, DHEA may bind in a different orientation to SULT-2A3.

3.3. Crystallographic dimer

The two monomers in the asymmetric unit A and B form the largest surface contacts in the unit cell. The overall buried surface area for the dimer is 1837 Å^2. These two molecules are related by a rotation of 170° from molecule B to molecule A along an axis nearly perpendicular to both the five-stranded β sheet and helix 6 (Fig. 5). Residues Met16–Lys19, Lys64–Glu73, Glu81–Glu91 and Lys227–Tyr238 of both molecules line the dimer interface. The orientation of residues Lys64–Glu73 in one molecule appears to lock the loop containing Tyr231–Gln244 of the other molecule, in a conformation which does not allow the substrate to bind. This is consistent with the fact that there is no electron density for DHEA even though the crystal was soaked in a buffer saturated with DHEA.

A crystallographic dimer is also observed in the SULT1A3 crystal structures [5,6]. Although the same surface of both monomers appear to be involved in the dimer contacts as with SULT2A3, the relative orientation of the second molecule of the SULT1A3 dimer differs from that of the SULT-2A3 second molecule by a crude rotation of about 110°. The calculated buried surface area for this crystallographic dimer is 1222 Å^2. The main residues involved in the dimer interactions are residues Val84–Pro90 and Phe142–His149. In the SULT1A3 crystals, the residues corresponding in sequence to Tyr231 –Gln244 of SULT2A3 are disordered. The loop containing residues Val84–Pro90 from the SULT1A3 molecule is shifted into the substrate binding pocket of the other monomer, occupying the position of loop Tyr231–Gln244 in the SULT2A3 structure and also appearing to disrupt substrate binding [5,6].

Consistent with previous studies [17], our purified recombinant SULT2A3 was active as a dimer (unpublished observation) and SULT1A3 is also reported to function as a dimer [6]. Thus, these common structural features in the crystallographic dimers suggest these crystallographic dimers may represent physiological dimers in an inactive state.

4. Conclusion

The crystal structure of SULT2A3 is the first determined for the SULT2 subfamily. It provides further evidence that the overall structures of the sulfotransferase family are well conserved. Analysis of crystal structures of SULT2A3 and SULT1A3 has revealed a common dimerization interface between the two molecules, implying that this interface might be general for cytosolic enzymes in solution. The interface interactions collapse the substrate binding pockets in the crystals of SULT2A3 and SULT1A3. Currently, biochemical and physicochemical approaches are being employed to investigate the physiological significance of these interactions. If the pockets were also collapsed in solution, our present structure presents a template for future research to describe the activation of enzymes.

Acknowledgements: We thank Dr. Y. Kakuta for his involvement in an early stage of this work. Our appreciation is also due to Dr. Mike Duffel for helping us to understand a monomer–dimer concept of sulfotransferases. We thank Dr. Z. Dauter, Dr. T. Transue and Dr. J. Krahn for helpful discussions on data collection, processing and refinement, and Dr. T. Hall and Dr. L. Pedersen for critical reading of the manuscript.

References

[1] Siiteri, P.K. and MacDonald, P. (1966) J. Clin. Endocrinol. Metab. 26, 751–761.
[2] Falany, C.N. (1997) FASEB J. 11, 206–216.
[3] Parker, C.R., Jr. (1999) Steroids 64, 640–647 and references therein.
[4] Kakuta, Y., Pedersen, L.G., Carter, C.W., Negishi, M. and Pedersen, L.C. (1997) Nature Struct. Biol. 4, 904–908.
[5] Bidwell, L.M., McManus, M.E., Gaedigk, A., Kakuta, Y., Negishi, M., Pedersen, L. and Martin, J.F. (1999) J. Mol. Biol. 293, 521–530.
[6] Dajani, R., Cleasby, A., Neu, M., Wonacott, A.J., Jhoti, H., Hood, A.M., Modi, S., Hersey, A., Taskinen, J., Cooke, R.M., Manchee, G.R. and Coughtrie, M.W.H. (1999) J. Biol. Chem. 274, 37862–37868.
[7] Kakuta, Y., Sueyoshi, T., Negishi, M. and Pedersen, L.C. (1999) J. Biol. Chem. 274, 10673–10676.
[8] Sueyoshi, T., Kakuta, Y., Pedersen, L.C., Wall, F.E., Pedersen, L.G. and Negishi, M. (1998) FEBS Lett. 433, 211–214.
[9] Comer, K.A., Falany, J.L. and Falany, C.N. (1993) Biochem. J. 289, 233–240.
[10] Navaza, J. (1994) Acta Cryst. A 50, 157–163.
[11] Brunger, A.T., Adams, P.D., Clore, G.M., DeLano, W.L. and Gros, P. (1998) Acta Cryst. D 54, 905–921.
[12] Otwinowski, Z. and Minor, W. (1997) Methods Enzymol. 276, 307–326.
[13] Jones, T.A., Zou, J.Y., Cowan, S.W. and Kjeldgaard, M. (1991) Acta Cryst. A 47, 110–119.
[14] Kakuta, Y., Peterotchenko, E., Pedersen, L.C. and Negishi, M. (1998) J. Biol. Chem. 273, 27325–27330.
[15] Marolais, F. and Varin, L. (1995) J. Biol. Chem. 270, 30458–30463.
[16] Petrotchenko, E.V., Doerflein, M.E., Kakuta, Y., Pedersen, L.C. and Negishi, M. (1999) J. Biol. Chem. 274, 30019–30022.
[17] Ogura, K., Shotome, T., Sugiyama, A., Okuda, H., Hiratsuka, A. and Watanabe, T. (1990) Mol. Pharmacol. 37, 848–854.
[18] Kraulis, P.J. (1991) J. Appl. Cryst. 24, 940–950.
[19] Merritt, E.A. and Bacon, D.J. (1997) Methods Enzymol. 277, 505–524.